

RESEARCH REPORT

Sipunculan celomocytes increase the resistance to H₂O₂-induced cell death under hypoxia**T Lombardo^a, DM Peralta^a, L Kornblihtt^b, GA Blanco^a**^aLaboratorio de Inmunotoxicología (LaITo), IDEHU-CONICET, Hospital de Clínicas, José de San Martín, Universidad de Buenos Aires (UBA), Buenos Aires, Argentina^bServicio de Hematología, Hospital de Clínicas, José de San Martín (UBA), Buenos Aires, Argentina

Accepted March 4, 2014

Abstract

Themiste petricola is a marine intertidal endolithic worm that experiences transient hypoxia within its habitat, owing to natural sediment movements or increased organic enrichment. We characterized and quantified the cytotoxic effect of H₂O₂ in celomocytes of the sipunculan *Themiste petricola* under normoxia and hypoxia (O₂ < 0.1 %) through the median effect method. The 50 % cell death H₂O₂ dose at 24 h (EC50) under normoxia was 1.5 mM. The range EC10-EC90 was 0.6 mM - 3.9 mM. The fraction of cells having collapsed mitochondrial membrane potential (MMP) was increased dose-dependently after 3 h exposure with 24 h cytotoxic doses of H₂O₂ from EC10 to EC90. The 24 h cytotoxic dose inducing 50 % of cells with collapsed MMP at 3 h was 3.67 mM. Intracellular superoxide anion production was increased dose-dependently, while reduced glutathione was decreased dose-dependently at 3 h with H₂O₂ from EC10 to EC90. Exposure to 24 h hypoxia did not cause cell death but induced intracellular acidification. The 24 h EC50 of H₂O₂ under hypoxia was increased to 4.7 mM while the range EC10-EC90 was increased to 0.9 mM - 25.1 mM. We conclude that hypoxia induces anaerobic metabolism and increases tolerance to H₂O₂-induced cell death in celomocytes of *Themiste petricola* preserving the immune functions and providing an advantage to survive under low oxygen tension.

Key Words: Sipunculans; hypoxia; hydrogen peroxide; ROS; cell death; median effect; celomocytes; Polychaetes; marine worms

Introduction

Sipuncula is a phylum of unsegmented marine celomate worms closely related to the polychaete annelids (Cutler 1994; Kristof *et al.*, 2008; Schulze and Rice 2009). *Themiste petricola* is an endolithic intertidal sipunculan species found within sedimentary rocks of variable grades of cohesion (Amor *et al.*, 1991). Most of sipunculan taxa came into existence in Paleozoic and Mesozoic times, when oxygen reached near-modern values and this has been suggested to explain why animals radiated so dramatically beginning at about 540 million years (Payne *et al.* 2011; Sperling *et al.*, 2013). While intertidal environments may be temporarily deprived of accessible oxygen, sipunculans are oxyconformants and may reduce

metabolic rate and energy demand as part of an adaptive response to hypoxia. The oxygen consumption of *Sipunculus nudus* conforms to the ambient oxygen tension (Portner *et al.*, 1985) and the same is true for *Themiste cymodoceae* and *Phascolopsis gouldi* (Edmonds 1957). However sipunculans can also revert to anaerobic pathways and live without oxygen for several days, producing lactic acid as one of the end products of metabolism (Edmonds, 1957).

Sipunculans have a celomic cavity filled with abundant red cells known as hemerythrocytes carrying the respiratory pigment hemerythrin and leukocytes mainly involved in innate immunity. Collectively these cells are also named celomocytes (Cutler, 1994; Blanco, 2010). Sipunculans are devoid of a circulatory and a respiratory system, but movements of the celomic fluid through activities of the animal and circulation in the tentacular system accomplish the functions of circulation and respiration (Cavaliere *et al.*, 2010). In ordinary conditions of sipunculan life, the hemerythrin is nearly completely saturated with oxygen, and hence

Corresponding author:

Guillermo A. Blanco

Laboratorio de Inmunotoxicología (LaITo)

IDEHU - CONICET - UBA

Junin 956 4to piso

Capital Federal (1113), Argentina

E-mail: gblanco@ffybu.uba.ar

is well adapted to the needs of the animal.(Hyman, 1959; Meyer and Lieb, 2010).

Oxidative stress is defined as an imbalance between oxidants and antioxidants which results in an excess of oxidative species (ROS) that leads to disruption in signalling, redox control, and molecular damage (Sheehan and McDonagh, 2008). When pro-oxidants and antioxidants are in a steady state, ROS are involved in intra and intercellular communication, and when the equilibrium is shifted towards pro-oxidants the damage to intracellular constituents ensues (Comhair and Erzurum, 2002; Speakman and Selman, 2011). Environmental pollutants including heavy metals, polycyclic aromatic hydrocarbons, and polychlorinated biphenyls have the potential to cause oxidative stress in aquatic organisms through ROS mechanisms (Sheehan and McDonagh, 2008). Aquatic organisms can uptake pollutants that cause oxidative stress damage from sediments and food sources (Valavanidis *et al.*, 2006). Marine invertebrates, especially bivalve mollusks, have been used extensively as sensitive bioindicators for aquatic pollutants associated with ROS generation (Chora *et al.*, 2008; McDonagh and Sheehan, 2008).

Hypoxia is a known source of oxidative stress in vertebrate cells (Lushchak and Bagnyukova, 2007). For example, hypoxia caused a dose-related increase in ROS production in cardiac myocytes (Duranteau *et al.*, 1998) and mammalian cell lines (Chandel *et al.*, 1998). In animals with closed circulatory system hypoxia-induced ROS facilitates a rapid microvascular inflammatory response characterized by enhanced leukocyte-endothelial adherence and emigration, which increases vascular permeability (Wood *et al.*, 1999; Peng *et al.*, 2003). Additionally ROS may be involved in defence against pathogens during phagocytosis (oxidative burst) (Fuller-Espie *et al.*, 2010). Even though hypoxia causes increased ROS several antioxidant mechanisms are also increased together with metabolic changes to increase anaerobic respiration (Lushchak and Bagnyukova, 2007).

Mitochondrial respiration, where oxygen is the final acceptor of electrons, is the main source of ROS, and superoxide anion (O_2^-), hydroxyl radical and hydrogen peroxide (H_2O_2) are produced even under normal metabolism. Superoxides are relatively unstable, with a half-life of only milliseconds, and do not easily cross cell membranes although it may cause damage to amino acids or loss of protein function (Valko *et al.*, 2007). The most harmful result of excessive intracellular ROS production is cell death. Most often cell death is initiated in the mitochondria where ROS concentration may be five to ten times higher than the cytosol (Cadenas and Davies, 2000).

Peroxidation of mitochondrial lipids compromises the normal function of the electron transport chain (ETC) leading to lower mitochondrial membrane potential (MMP) and altered regulation of Ca^{2+} . This in turn may initiate programmed cell death (Zhang *et al.*, 1990). Although H_2O_2 is not a free radical, it is an extremely harmful ROS because it acts as an intermediate in hydroxyl radical producing reactions, such as Fenton's reaction

Table 1 Cytotoxic doses of H_2O_2 in celomocytes

Effect level (EC%) at 24h	Normoxia	Hypoxia
	H_2O_2 (mM)±SE N=24; n=20000(*)	H_2O_2 (mM)±SE N=24; n=20000(*)
EC10	0.58±0.04	0.89±0.05
EC30	1.05±0.07	2.48±0.10
EC50	1.52±0.10	4.72±0.31
EC70	2.19±0.17	8.99±0.92
EC90	3.94±0.41	25.07±4.15
EC95	5.45±0.66	44.23±8.94
EC98	11.17±1.83	154.97±44.57

(*) n is the number of cells used to determine the fraction of dead cells per sample; N is the number of samples used for regression analysis.

(Koppenol, 2001). H_2O_2 has a long half-life and is able to cross several lipid layers and react with transition metals and some hemoproteins (Miller *et al.*, 2010). It can also induce DNA damage, chromosomal alterations, and oxidize sulfhydryl compounds (Cantoni *et al.*, 1989). When H_2O_2 is added experimentally at increasing doses, an active programmed cell death is elicited while higher doses will induce passive necrosis (Jiang *et al.*, 2013). In vertebrate cells active cell death by excess oxidative damage caused by H_2O_2 is initiated at the mitochondria (Luo *et al.*, 2010; Palomba *et al.*, 1999). This is similar to the cytotoxic mechanism of several xenobiotics including heavy metals and pesticides that target the mitochondria and cause abnormal function of the ETC with increased ROS production, decreased MMP and initiation of cell death (Wang *et al.*, 2012).

We have previously shown that H_2O_2 induces apoptotic-like cell death in celomocytes of *T. petricola* (Blanco *et al.*, 2005). However the celomocyte population includes cell types such as hemerythrocytes and leukocytes that may exhibit differential sensitivity over a range of H_2O_2 doses. In this study we assessed the whole range of cytotoxic effects of H_2O_2 in celomocytes by the median effect method, which is basically a log-transformed regression method where parameters of a sigmoid dose-response curve are estimated (Chou, 2011; Lombardo *et al.*, 2012, 2011). We also characterized the early effects caused by H_2O_2 exposure including mitochondrial damage, ROS production and anti-oxidative response in normoxia, and we further evaluated the cytotoxic effect of H_2O_2 in celomocytes under hypoxia.

Materials and methods

Worms

Adult *Themiste petricola* were collected from crevices in intertidal rocks at Santa Elena beach on the coast of Argentina (34°S latitude) and maintained in plastic boxes with frequently renewed filtered sea water with 32 parts per thousand (ppt) salinity at 18 °C. The salinity of the sea water that the subject worms were originally found in was 32 ppt. Celomocyte suspensions were prepared as indicated previously (Blanco *et al.*, 2005). Briefly, celomic fluid was harvested by incision of the body wall with a sterile surgical blade, allowing the fluid to drip into a 15 ml tube. Germinal cells were excluded with sterile filters of 30 µm mesh. The suspension was washed two times by centrifugation in a saline solution made of 26g/L NaCl (890 mOsm; 0.444 M NaCl) with 5 % sea water (v/v). Addition of 5 % sea water depletes celomic fluid from large and small granular leukocytes by forming a small but macroscopic clot (Blanco, 2010), while washing in 0.4 M NaCl alone preserves both types of granular cells. The cell suspension was washed once more in RPMI-1640 (Invitrogen, Argentina) supplemented with L-glutamine, 17g/L NaCl, and sodium bicarbonate pH 7.4 (900 mOsm/kg). All subsequent references to RPMI correspond to this modified culture medium.

Reagents and in vitro culture of celomocytes

Fresh stock solutions of H₂O₂ were prepared for each experiment. Fluorescein-diacetate (FDA), dihydroethidine (HE), tetramethylrhodamine-ester (TMRE), 5-chloromethylfluorescein (5CMF), 4',6'-diamidine-2-phenylindol (DAPI) and propidium iodide (PI) were purchased to Invitrogen. The stock solutions of HE and PI were prepared in DMSO and the rest in phosphate buffer saline (PBS, 295 mOsm).

Assessment of cell death

Celomocytes harvested from five to ten worms as described above were suspended in RPMI and decanted in 24-well culture plates 1.0x10⁶ per well in 0.5 ml. Serial dilutions of H₂O₂ in 0.5 ml RPMI were added in triplicate. RPMI (0.5 ml per well) was added as untreated control in triplicate. Experiments were repeated widening, narrowing or shifting the dose ranges and intervals between doses until a suitable scheme was found to cover the entire effect range (*i.e.*, from no cytotoxic effect to maximal cytotoxic effect). This was necessary because the median effect method requires experimental values of cytotoxicity to cover the entire range of effects from no effect (negative control) to 100 % effect (maximum positive effect control) with sufficient intermediate values to obtain statistically precise estimates of the slope (m) and intercept (- m . log[Dm]) parameters in a log-linear regression (see description of the median effect method in the section below). The plates were incubated for 24 h at 18 °C. To identify dead and live cells samples were incubated in 1 µM FDA in RPMI for 15 min, washed three times in NaCl 0.4M by centrifugation at 300xg during 5 min at RT, transferred to flow cytometry tubes, stained with 2 µM PI for 5 min in

1ml NaCl 0.4M, and run in a Partec PAS III flow cytometer equipped with a 100 W UV-mercury lamp source light and a 20 mW 488 argon laser (Partec, GmbH, Münster, Germany). A total of 20,000 events were analyzed per sample tube containing 1 x 10⁶ cells in 1 ml of 0.4M NaCl. Each sample tube corresponded to cells harvested from each well of a 24-well plate. The FDA and PI fluorescence were collected through a 535/15 nm and 680/15 bandpass filter respectively. Quadrant analysis was done with Flomax software (Partec, Germany) and WinMDI 2.8 (Scripps Research Institute, La Jolla, CA, USA).

Median-effect and combination index analysis of cytotoxicity

Live vs. dead discrimination at the single cell level through flow cytometry allowed us to use a quantal dose-response model where *Fa* was the fraction of dead cells (obtained from the percentage of cells in upper quadrants of flow cytometry dot plots) while *Fu* was the fraction of live cells and $Fu = (1-Fa)$ (Lombardo *et al.*, 2012). We further created a median-effect plot as log (*D*) vs. log (*Fa/Fu*), where *D* was the dose of H₂O₂ in each experimental sample point (each well of a 24-well culture plate). By linear regression we obtained the slope and the intercept estimates of the equation $\log(Fa/Fu) = m \cdot \log(D) - m \cdot \log(Dm)$ to further derive the estimate of the median effect dose (*Dm*). With the slope *m* and the median effect dose *Dm* we derived the median effect formula for H₂O₂:

$$D=Dm (Fa/(1-Fa))^{1/m}$$

With this formula we could further estimate the dose *D* of H₂O₂ that induces cytotoxicity in a fraction *Fa* of cells in a 24 h incubation experiment. Thus we refer to the *Fa* value as cytotoxic effect level (EC), and we denote the estimated dose *Dm* that kills 50 % of cells (*Fa* = 0.5) in a 24 h assay as EC50 %. In the same way a dose *D* that according to the formula is estimated to kill 30 % of cells (*Fa* = 0.3) in a 24 h assay is referred to as EC30 and so on for any arbitrary cytotoxic effect level. The same method was used to determine the dose *D* of H₂O₂ that causes the collapse of mitochondrial membrane potential in a 3 h assay, and that we refer to as ED. In this case the fraction *Fa* was derived from the percentage of cells with complete collapse of the MMP, which in turn was obtained from histograms of each of the replicates. Further details of the median effect method can be found in (Chou, 2011; Lombardo *et al.*, 2011, 2012). Calculations were performed with the software Calcsyn (Biosoft, UK). The SE of EC% values were calculated with Calcsyn software according to the following formula (Lombardo *et al.*, 2012):

$$SE(D) = 1/2 \cdot \{10^{[\log(D)+SE(\log(D))]} - 10^{[\log(D)-SE(\log(D))]} \}$$

where:

$SE(\log(D)) = \{[\log(D) \cdot [SE(b)/\log(fa/(1-fa)-b)]^2 + [SE(m)/m]^2 + 2[-(\log(D))^{1/2} \cdot SE(m)/SE(b)]] \cdot SE(b)/b \cdot SE(m)/m\}^{1/2}$, and $b = -m \cdot \log(Dm)$, $Dm=EC50$, and $D=EC\%$ for each particular effect level.

Assessment under hypoxia

To assess the effect of H₂O₂ under hypoxia the culture plates were prepared as described above and were further placed in a MIC-101 chamber (Bilrups Rothemberg, USA), connected to a dual flow meter that supplied a gas mixture containing 95 % N and 5 % CO₂. Under such conditions the chamber is designed to keep O₂ concentrations below 0.1 % when flushed for at list 10 min.

Evaluation of reduced glutathione (GSH) intracellular content

After exposing celomocytes to H₂O₂ for the appropriate time they were washed by centrifugation at 300xg during 5 min at RT in 1 ml of 0.4M NaCl to avoid the interference of thiol groups that could be present in the RPMI medium, and were further incubated in 0.3 μM 5CMF in 1 ml of 0.4M NaCl during 20 min at RT. This probe becomes fluorescent in live cells and then binds covalently to GSH with high specificity (Sarkar *et al.*, 2009). Cells were washed once more at 300xg during 5 min at RT in 1 ml of 0.4M NaCl and then PI was added at a final cc of 2 μM in 0.4 M NaCl to obtain an additional and independent parameter of cell death.

Assessment of O₂⁻ production and statistical analysis

HE, a probe that is oxidized to ethidium by intracellular O₂⁻ (Chen *et al.*, 2009) was prepared as a 5 mM stock solution in DMSO and stored at -70 °C. A 500 μM working solution was prepared by diluting 1/100 the stock solution in 0.4 M NaCl. After exposure to H₂O₂ in 3 h assays cells were washed and incubated during 20 min at RT with HE 2 μM final concentration. Cells were washed again by centrifugation at 300xg during 5 min at RT in 1 ml of 0.4M NaCl and further analyzed by flow cytometry. Fluorescence of a positive control made by exposing a sample of cells to 50 μM carbonyl cyanide m-chlorophenyl hydrazone (CCCP; Sigma-Aldrich) in 1 ml of 0.4M NaCl 10 min prior to adding the HE probe, and basal fluorescence of non-treated samples were used as reference to compare changes induced by H₂O₂ treatment.

Assessment of mitochondrial membrane potential (MMP)

Celomocytes were treated with H₂O₂ during different time intervals at a fixed EC50 dose or at a fixed time interval of 3 h at increasing doses of H₂O₂ in 24-well culture plates (1x10⁶ per well in 1 ml RPMI) at 18 °C. Each dose or time point was assessed in triplicate. The cells from each well were further transferred to microcentrifuge tubes and centrifuged at 300xg at RT during 5 min. The supernatant was discarded and the cells were suspended 1 ml of NaCl 0.4 M with the potentiometric probe TMRE 0.05 μM final cc during 30 min. A positive control was included by treating a sample of cells (1x10⁶ in 1 ml of 0.4 M NaCl) during 10 min with the mitochondrial electron transport chain uncoupler CCCP (50 μM final cc). This treatment, which was applied prior to labelling with TMRE, causes complete collapse of MMP and serves as a positive control of depolarizing effect. The untreated samples with normal MMP served as

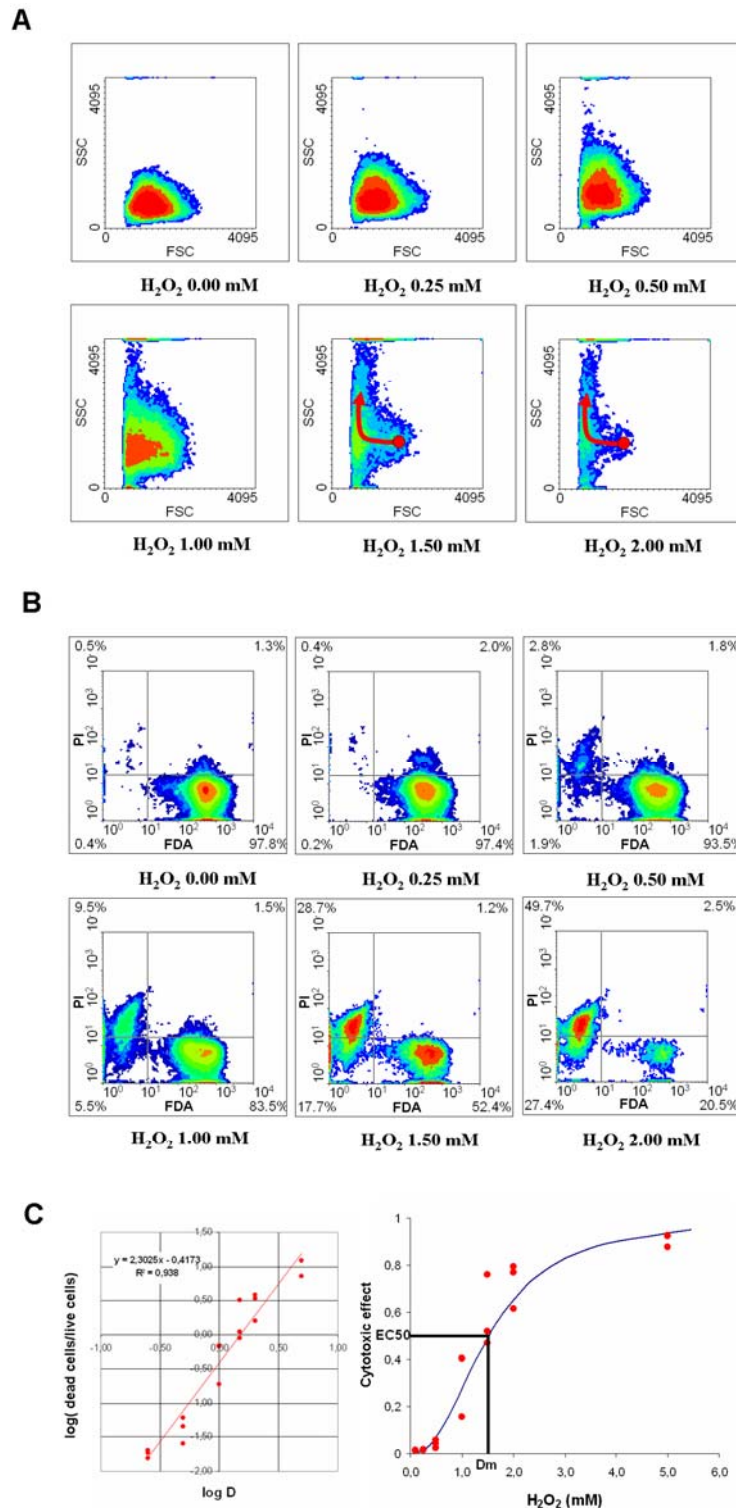
negative controls or baseline of depolarizing effect. After labelling cells with the probe TMRE cells were washed by centrifugation at 300xg at RT in 1 ml 0.4 M NaCl. The cells were finally suspended in 1 ml NaCl 0.4 M, transferred to flow cytometry tubes and analyzed by flow cytometry. A total of 20,000 events were acquired from each of the 24 tubes.

Assessment of phagocytosis

Zymosan particles (Sigma) were suspended at 1 mg/ml in 0.4 M NaCl and labelled with DAPI 10 μg/ml final cc at RT during 1 h. This suspension was washed three times by centrifugation at 900xg in 0.4 M NaCl during 5 min at RT. Celomocytes were incubated in 24-well culture plates with these labelled particles at three time intervals (1 h to 3 h) and two concentrations (250 μg/ml and 500 μg/ml). To assess production of O₂⁻ during phagocytosis the samples were further incubated with HE as described in the correspondent section above. A sample of celomocytes was exposed to EC90 H₂O₂ (3.9 mM) for 18 h at 18 °C to obtain a preparation of cells undergoing cell death. These cells were labelled with 10 μg/ml DAPI in RPMI. A separate sample of untreated cells was suspended at 1x10⁶/ml in RPMI with 1 μM FDA and incubated for 15 min at 18 °C. These cells were washed three times in RPMI by centrifugation at 300xg during 5 min at RT and decanted into a 24-well culture plate at 1x10⁶ per well in 0.5 ml. The DAPI-labelled cells were added at 1x10⁶ per well in 0.5 ml and the co-culture was incubated for another 4h to allow live FDA-stained cells to phagocytose DAPI-stained dead cells. After incubation the samples were transferred to flow cytometry tubes then analyzed with dual 360 nm UV and 488 nm blue excited flow cytometry. Additional controls included FDA-stained cells without DAPI-stained cells, DAPI-stained cells without FDA-stained cells, DAPI-labelled zymosan particles and unlabelled zymosan particles. A total of 20,000 events were acquired from each flow cytometry tube containing more than 1x10⁶ cells in 1 ml.

Statistical analysis

Flow cytometry histograms or bivariate plots were analyzed using multiparametric gating with the software WinMDI 2.8 (Scripps Research Institute, La Jolla, CA, USA). The frequency values of cell death were obtained from quadrant analysis of FDA vs. PI plots in triplicates (20,000 cells acquired per sample) for each of the doses tested. The frequency values of cells with complete collapse of MMP were obtained from TMRE fluorescence histograms in triplicates (20,000 cells acquired per sample) for each of the doses tested. These data were further used in a log-transformed regression as indicated in the correspondent section above. For statistical analysis of fluorescence intensity the original log-fluorescence data were exported with WinMDI software to Graph Pad Prism 4.0 software (GraphPad, San Diego, USA). We applied the non-parametric Kruskal-Wallis test for differences between fluorescence medians among all treatments followed by Dunn's post hoc test to evaluate differences of the medians between treated and non-treated samples (Lombardo *et al.*,



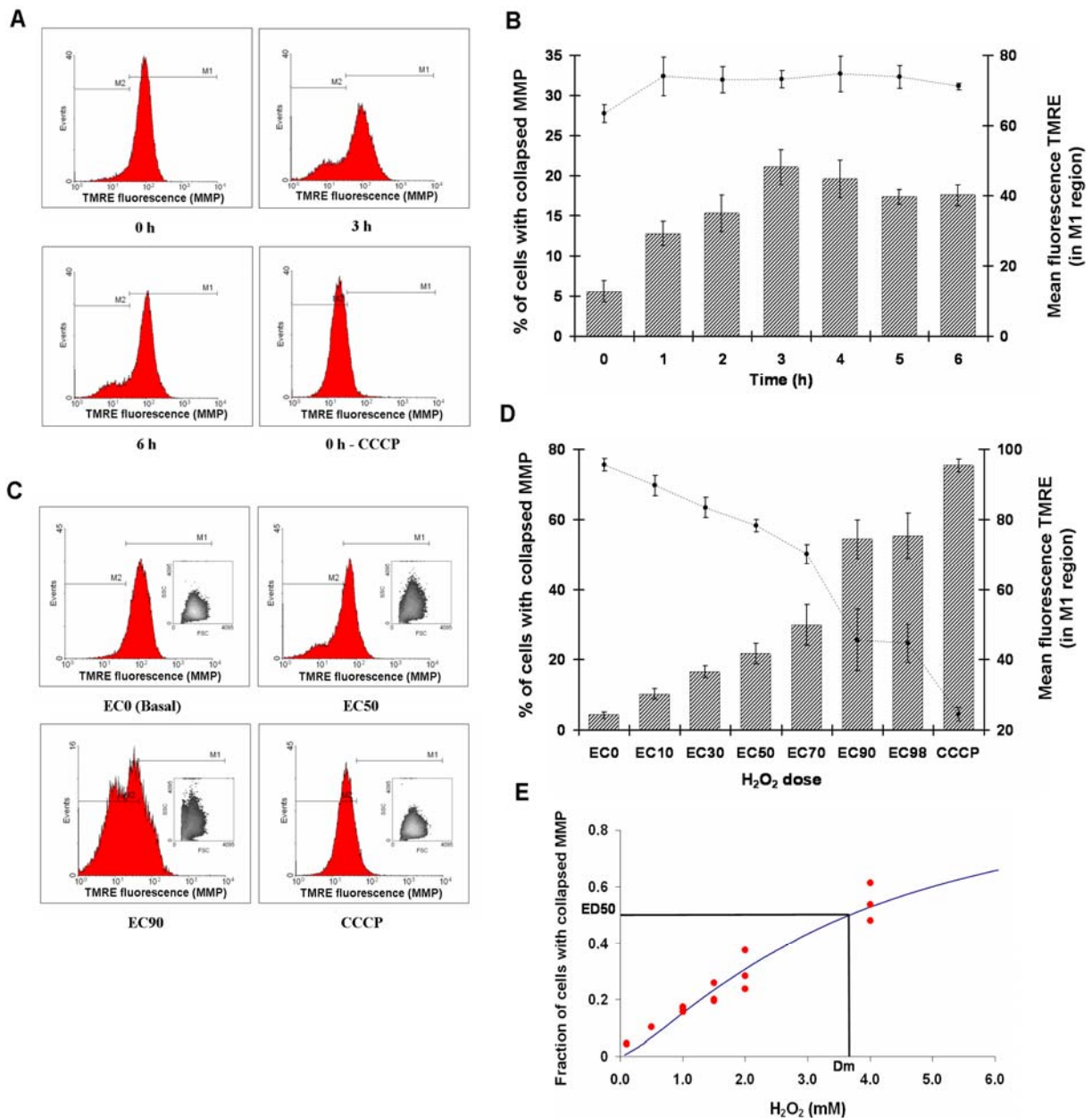


Fig. 2 Evaluation of MMP after exposure of celomocytes to H₂O₂. A) Effect of EC50 H₂O₂ at increasing time intervals (up to 6 h). Representative histograms of cells labelled with the potentiometric probe TMRE and assessed at increasing time points are shown. M1 refers to the region of cells having a positive MMP while M2 refers to the region of cells with collapsed MMP. The histogram labelled 0h-CCCP corresponds to a positive control of complete collapse of MMP made of untreated cells exposed to the mitochondrial ETC uncoupler CCCP and used to accurately define the M2 and M1 regions. The histogram labelled 0h is a negative control of complete collapse of MMP and is a baseline corresponding to the normal MMP of untreated cells B) Bar graph showing that the percentage of EC50 H₂O₂-treated cells with collapsed MMP (cells in M2) increased with time length up to 3 h when it achieved a plateau (scale on left axis). Dots correspond to the mean TMRE value (from triplicates) of cells that still kept a positive MMP (cells in M1 region) and the scale is shown on the right axis. Error bars around dots or grey bars correspond to the mean value \pm SD of triplicates. C) Representative histograms of cells treated with increasing doses of H₂O₂ and evaluated after 3 h for TMRE fluorescence. Insets show FSC-SSC density plots to appreciate the shape changes after 3 h exposure. D) Bar graph showing that the amount of cells with collapsed MMP increased with increasing doses of H₂O₂ (left axis). In addition those cells that still kept a positive MMP showed a progressively decreased mean value of TMRE fluorescence (black dots with scale on right axis). Error line bars around dots or grey striped bars correspond to the mean value \pm SD from triplicates. For the actual H₂O₂ concentration of EC% values see Table1. E) Calculation of the H₂O₂ dose that causes MMP collapse at 3 h in 50 % of cells (ED50) applying a linear regression of log-transformed data and the median effect equation. A plot of the complete dose-effect equation (blue line) together with experimental values (red dots) is shown. See materials and methods section for additional details on the median effect equation and the calculation method.

2011). Box-Whisker plots were obtained with GraphPad Prism 4.0 as part of the exploratory data analysis to further visualize the H₂O₂-induced changes in fluorescence intensity frequency distribution. Correlation analysis between GSH content and superoxide anion production was conducted by calculation of the Pearson's r correlation coefficient with GraphPad Prism 4.0 software. Nonlinear regression was applied to a hyperbolic function of the type $y = k/x+b$ representing the inverse relationship between GSH and superoxide anion using Graph Pad Prism 4.0 software.

Results

Dose-related H₂O₂-induced cell death in sipunculan celomocytes

Celomocytes exposed to H₂O₂ over a range 0.25 mM to 5.0 mM during 24 h showed a dose-related increase in the amount of dead cells as determined by FDA and PI labelling and flow cytometry assessment. Increasing doses of H₂O₂ also caused changes in cell shape as indicated by forward and side light dispersion in flow cytometry bivariate plots (Figs 1A, B). At low effect doses within the range 0.25 mM to 1.0 mM H₂O₂ we observed an increase in the side scatter light parameter (SSC) of cells but at the same time only a slight increase in the fraction of dead cells which remained below 11 %. However at doses above 1.0 mM H₂O₂ both the fraction of dead cells and the SSC were increased while the forward light scatter (FSC) was decreased (Figs 1A, B). This profile became clearer when experimental values were used to calculate the H₂O₂ dose causing death in 50 % of cells (EC50 = 1.52 mM, SE = 0.10) and to obtain a sigmoid dose-effect curve (Fig. 1C).

The linear increase in cell death was observed between 1.0 mM and 2.0 mM (Fig. 1C). We presumed that the increase in SSC without increase in cell death at low H₂O₂ doses could be due to the fact that phagocytes, which may have a higher oxidative stress tolerance, could be engulfing dead cells (or even cells undergoing programmed cell death) that were sensitive to lower doses of H₂O₂. Thus we explored this possibility in a section below. As expected, the sigmoid shape and the steepness of the linear segment showed that there was a range of susceptibilities to H₂O₂-induced cell death among celomocytes, where some cells may be killed with 1.0 mM H₂O₂ while others may tolerate more than 2.0 mM H₂O₂. The actual H₂O₂ concentrations for EC% values derived from the median effect equation and used in the study are shown in Table 1.

Assessment of mitochondrial damage caused by H₂O₂ exposure

We further evaluated MMP through the potentiometric probe TMRE at several time points after exposing cells to the 24 h EC50 H₂O₂ (1.5 mM). The proportion of cells with collapsed MMP increased linearly up to 3 h and remained constant afterwards (Figs 2A, B). In addition those cells that still kept a positive MMP maintained stable and high polarization as indicated by a steady value of the

mean fluorescence of TMRE. We next evaluated the MMP at 3 h post-exposure at several doses of H₂O₂ ranging from EC0 to EC98. We observed a dose-dependent increase in the amount of cells with collapsed MMP and also a progressive decrease in MMP among those cells that still kept a positive MMP (Figs 2C, D). We next calculated the dose of H₂O₂ that causes the complete collapse of MMP in 50 % of cells (ED50 = 3.67 mM) by the method of the median effect equation, and we further obtained the parameters of a curve describing the relationship of H₂O₂ dose to MMP collapse at 3 h (Fig. 2E). Thus, by comparing this curve with the one in Figure 1C, the fraction of cells with collapsed MMP at 3 h can be used as a biomarker to forecast the amount of cell death that will be observed at 24 h.

Mitochondrial damage causes an increase in oxidative stress

The direct consequence of mitochondrial damage originated in the pulse of H₂O₂ is the failure of ETC and the production of ROS. The production of O₂⁻ was increased dose-dependently at 3 h in agreement with increased mitochondrial failure (Figs 3A, B). To evaluate if celomocytes attempted to reduce the impact of increased ROS production by means of an antioxidant response we measured the amount of intracellular GSH by the fluorescent probe 5CMF at 3 h, since GSH is one of the most ubiquitous and efficient cellular antioxidants. As expected, increasing doses of H₂O₂ caused a progressive decrease in the amount of GSH detected (Figs 4A, B). The amount of GSH detected was inversely correlated to the amount of intracellular O₂⁻, and also inversely correlated to the amount of cells showing complete collapse of MMP (Figs 4C, D).

Phagocytosis may contribute to eliminate potentially harmful damaged self cells

We evaluated the ability of celomocytes to phagocytose DAPI-stained zymosan particles. As shown in the left panel of Figure 5A cells unexposed to DAPI-stained zymosan had no blue fluorescence because no engulfment of fluorescent particles occurred. This sample represented a negative control or baseline of blue autofluorescence for comparison with cells exposed to DAPI-stained zymosan particles. In the right panel of Figure 5A cells that engulfed DAPI-stained zymosan particles appear above the baseline of blue autofluorescence. The fact that FSC of the zymosan-exposed cells had a similar distribution as untreated cells denotes that these cells had acquired the blue fluorescence by engulfing the already labelled DAPI-stained zymosan particles.

As shown in Figure 5B when celomocytes were exposed to DAPI-stained zymosan the highest amount of intracellular particles was detected after 1 h and decreased progressively at 2 h and 3 h. In addition at the 1 h time point the phagocytosis of DAPI-stained zymosan particles was coincident with an increase in O₂⁻ production as detected by the simultaneous presence of DAPI-stained zymosan particles (blue fluorescence) and increased HE fluorescence by flow cytometry (Fig. 5C). Therefore,

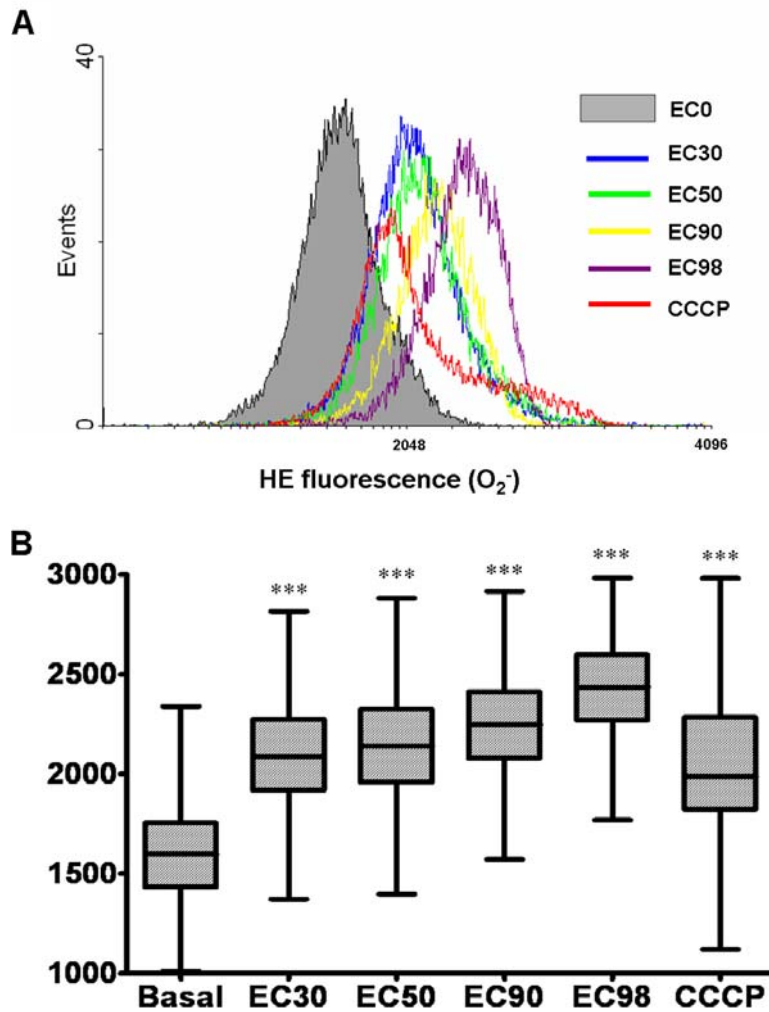


Fig. 3 Assessment of intracellular O₂⁻ production after 3 h incubation at 18 °C with increasing doses of H₂O₂. A) Overlaid histograms of cells treated with increasing doses of H₂O₂ and evaluated after 3 h for HE fluorescence indicating the amount intracellular O₂⁻ production. B) Box whisker plots of the samples shown in A. Data from 20,000 events from each sample were exported to the software GraphPad Prism 4.0 for further statistical analysis. Median values were compared by the non-parametric Kruskal-Wallis test with significance $p < 0.001$ and median values of H₂O₂-treated samples and the CCCP control were compared to untreated cells using Dunn's post test for median differences. ***: $p < 0.001$ for difference with median of untreated cells in Dunn's post test. Whiskers represent ± 1.5 inter-quartile distance (IQD) (Le Meur *et al.*, 2007).

among celomocytes exposed to H₂O₂ the phagocytes could be the more resistant ones and could also be responsible for eliminating the more sensitive cells that undergo cell death at the lower doses. To provide some evidence to this hypothesis we exposed cells to H₂O₂ at a high dose (EC90) during 18 h. We then labelled these cells with DAPI, and we further incubated these dead cells during 4h more with live cells that were previously labelled with FDA to make them green fluorescent. As shown in Fig. 6A live and dead cells had completely different FSC vs. SSC profile. We then identified the amount of live cells that had engulfed dead cells, the amount of cells that were alive but had not engulfed dead cells and the amount of dead cells that had not been engulfed and remained free (Figs

6B, C). This experiment proved that phagocytes can actively engulf dead cells and in fact it could be possible that they can also engulf cells that are still alive but undergoing a death program as a mean to eliminate a potential source of ROS and tissue damage. As shown in Fig. 6C those live cells that actively engulfed dead cells can exhibit an increase in SSC as was observed in Figure 1A.

H₂O₂-induced cell death is decreased under hypoxia

When celomocytes were exposed for 24 h to less than 0.1 % O₂ but in the absence of H₂O₂, they survived without any change in cell viability. However the culture media shifted to a strong yellow color indicating a rapid acidification of the extracellular media (data not shown), while the FDA

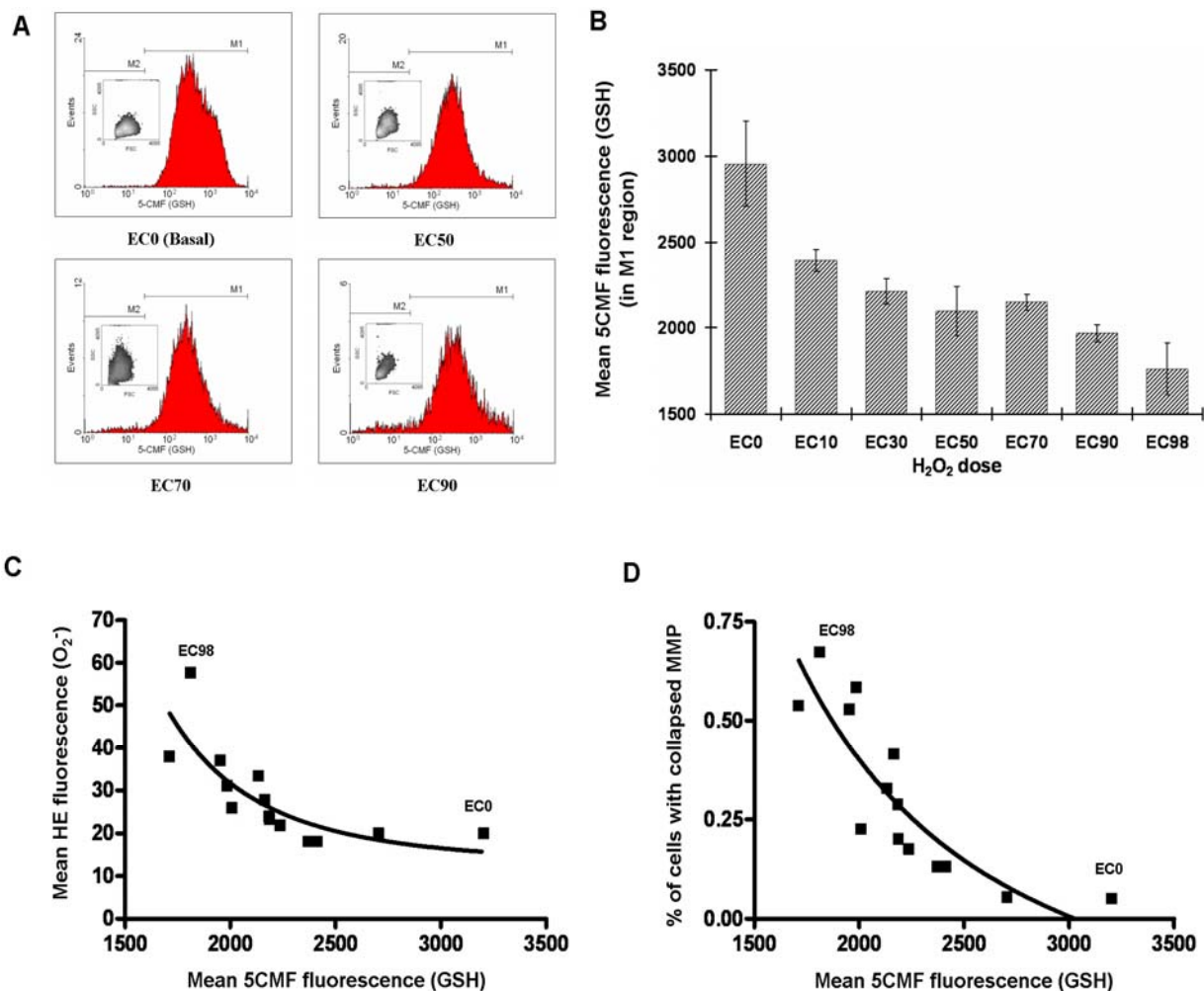


Fig. 4 Assessment of intracellular GSH level after 3 h incubation at 18 °C with increasing doses of H₂O₂. A) Representative histograms of cells treated with increasing doses of H₂O₂ and evaluated after 3 h with 5CMF to measure the level of intracellular GSH. Insets show FSC-SSC density plots of the same sample to appreciate the shape changes induced after 3h exposure. B) Bar graph showing that intracellular GSH decreases with increasing doses of H₂O₂ when evaluated after 3h. Error bars correspond to the mean value ± SD from triplicates. C) Correlation analysis of intracellular GSH content vs. intracellular O₂⁻ production. Pearson's correlation coefficient *r* was -0.67 with significance *p* < 0.05. The nonlinear regression curve representing the inverse relationship corresponds to a hyperbolic function of the type $y = k/x+b$ ($R^2 = 0.64$). D) Correlation analysis of GSH content vs. amount of cells with collapsed MMP having a Pearson's correlation coefficient of -0.80 with *p* < 0.001. The nonlinear regression curve also corresponds to a hyperbolic function of the type $y = k/x+b$ ($R^2 = 0.75$).

fluorescence intensity of hypoxic celomocytes was reduced indicating that the cytoplasm had also become acid (Figs 7A, B). The reduction of intensity was about 100 times and the reason why fluorescence decreases is that FDA light absorption at 488 nm is reduced depending on how low the intracellular pH is (Geisow, 1984; Martin and Lindqvist, 1975). This property has been used to measure intracellular acidification with FDA in nerve cells under intense glycolysis and high production of lactic acid (Khodorov *et al.*, 1994).

The EC₅₀ of H₂O₂ under hypoxia was increased to 4.72 ± 0.31 mM (mean ± SE estimated from linear regression of log-transformed data using the median effect equation), and the dose effect

curve was deviated to the right indicating that cells became more tolerant to oxidative stress as compared to the same doses applied under normoxia (Figs 7C - E). The EC% values for other cytotoxic effect levels under hypoxia are shown in Table 1. Of notice, in samples treated with H₂O₂ under hypoxia the FDA fluorescence was decreased but to a less extent than untreated samples (about 10 times reduction compared to 100 times reduction in untreated samples under hypoxia; Figs 7B - D). This acidification under severe hypoxia is known as "Pasteur effect" and is due to enhanced anaerobic glycolysis with overproduction of lactic acid. Thus, even though hypoxia may trigger antioxidant defences, H₂O₂ may also compromise the efficiency

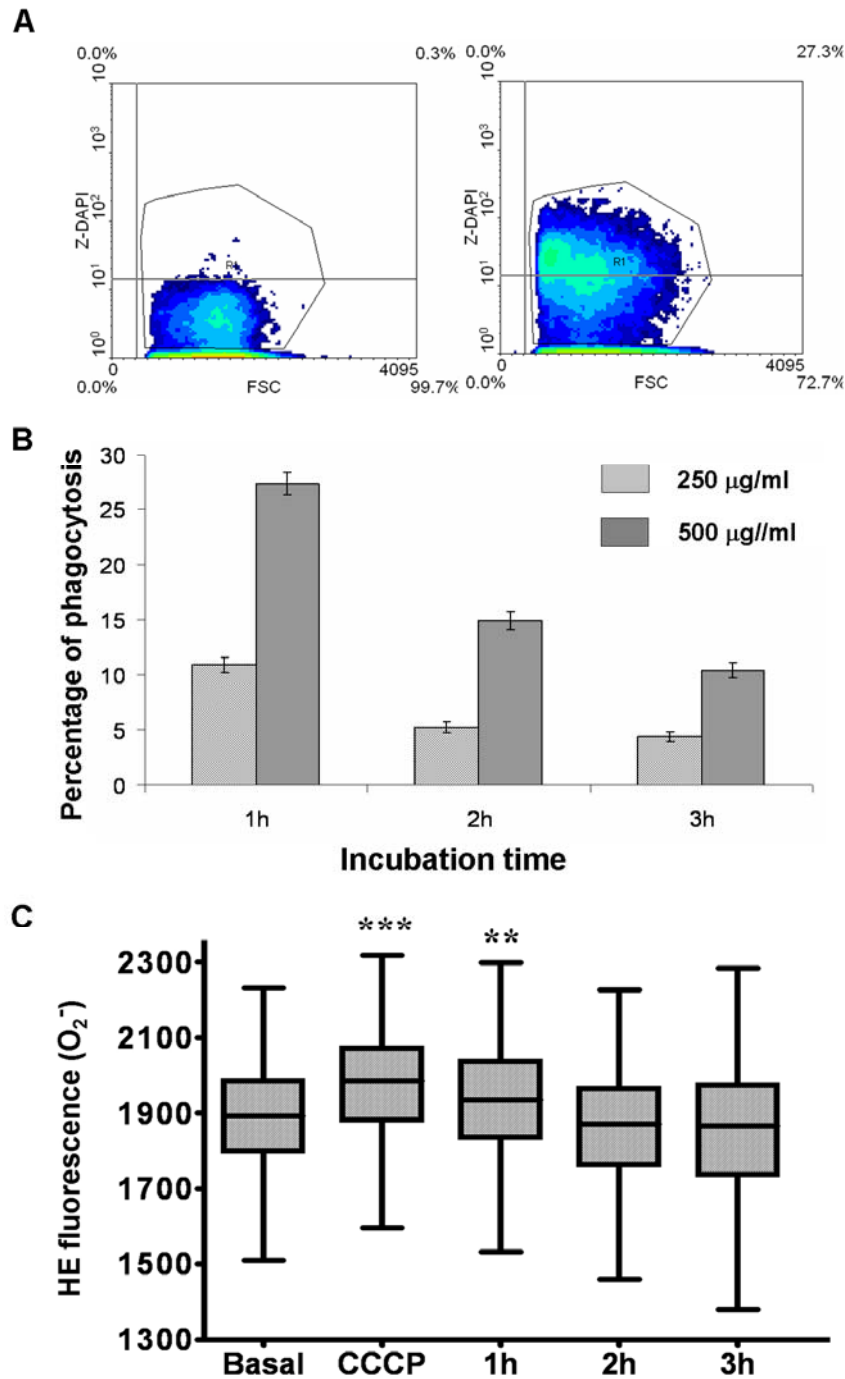


Fig. 5 Phagocytosis and oxidative burst in celomocytes exposed to zymosan. A) Phagocytosis of DAPI-stained zymosan particles by celomocytes. The left panel shows a negative control of phagocytosis where only baseline levels of blue fluorescence are present. In the right panel those cells that engulfed zymosan particles became blue-fluorescent (Z-DAPI y axis) and appear above the baseline of blue autofluorescence. The percentage of celomocytes above this value indicates the percentage of phagocytic cells. Free non-phagocytosed particles are excluded due to their low FSC signal. B) Phagocytosis of DAPI-stained zymosan particles by celomocytes evaluated at three time points and two concentrations of target particles. Bars indicate the mean value \pm SD of cells that engulfed fluorescent zymosan particles from triplicates. C) The median red fluorescence of HE indicating O₂⁻ production among cells that engulfed DAPI-stained zymosan particles (blue fluorescent) was computed as an indicator of the amount of intracellular oxidative burst during phagocytosis. Data from 20,000 events from each sample were exported to the software GraphPad Prism 4.0 for further statistical analysis. The Box-Whisker plot corresponds to cells exposed to 500µg/ml DAPI-stained zymosan and evaluated after 1, 2 and 3 h, with HE. CCCP corresponds to the positive control for O₂⁻ production. Treatments were compared with the non-parametric Kruskal-Wallis test with significance $p < 0.001$ and medians further compared by Dunn's post test. ***: $p < 0.001$ and **: $p < 0.01$ for differences with median of untreated cells in Dunn's post test. Whiskers represent ± 1.5 IQD (Le Meur *et al.*, 2007).

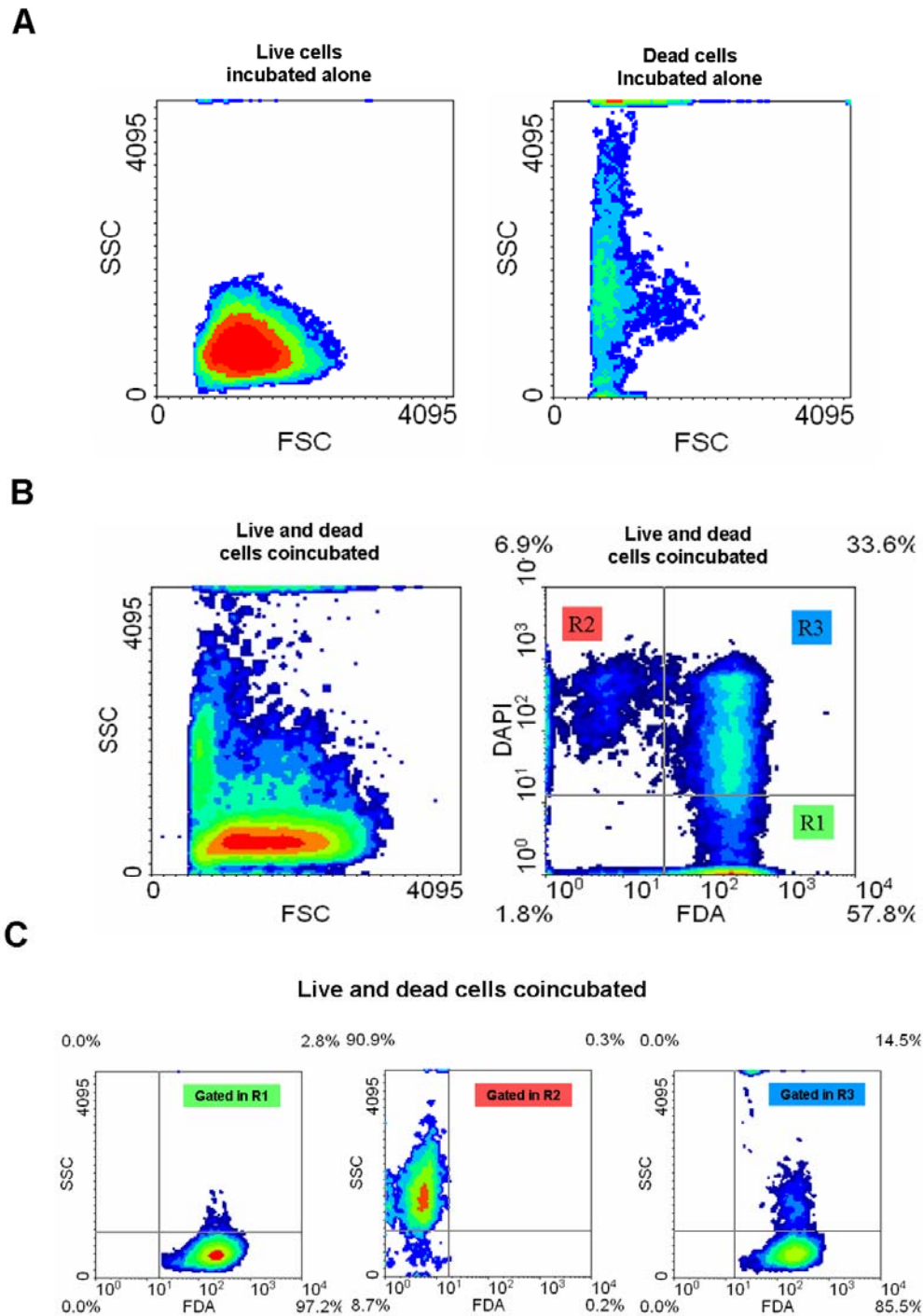


Fig. 6 Phagocytosis of dead celomocytes by live celomocytes. A) Density plots showing FSC and SSC in live untreated cells (left) and changes occurring in dead cells (right) after 18 h culture with EC90 H₂O₂ at 18 °C. B) The suspension of dead cells was labelled with DAPI, which is a nonpermeant dye excluded by live cells similarly to PI but has blue fluorescence, while the suspension of live cells was stained with FDA (green fluorescence of FDA indicates metabolic activity of viable cells) and then they were coincubated for 4 h at 18 °C. The left panel shows the FSC vs. SSC distribution of coincubated cells. The right panel shows the bivariate distribution of FDA vs. DAPI fluorescence that allows distinction of three clusters located in three separate regions R1, R2, and R3. Region R1 corresponds to live cells that did not engulf DAPI-stained dead cells and thus remain FDA single positive. Region R2 corresponds to DAPI-stained cells that were not engulfed. Region R3 corresponds to live cells (FDA positive) that have engulfed DAPI-stained dead cells and became blue fluorescent in addition to being green fluorescent (*i.e.*, double positive). C) Backgating of the three regions identified in B) applied to show the individual SSC characteristics of each group. Live cells that did not engulf dead cells have no change in SSC (R1, left panel). Dead cells that were not engulfed by live cells had increased SSC (R2, mid panel). The majority of live cells that engulfed DAPI-stained dead cells had no change in SSC (85.5 %) but a fraction of them showed increased SSC (14.5 %) corresponding to the most active phagocytic cells.

of anaerobic glycolysis. In addition the range EC10-EC90 was increased from [0.58 mM - 3.94 mM] under normoxia to [0.89 mM - 25.0 mM] under hypoxia (Table1) and the steepness of the linear part of the dose-response curve was decreased. The slope of the log regression was 2.32 under normoxia (Fig. 1C left panel) and was reduced to 1.30 under hypoxia (Fig. 7E left panel). This indicates that the variability in the susceptibilities to H₂O₂-induced cell death among celomocytes was also increased under hypoxia.

Discussion

In this study we characterized the dose-effect relationship of H₂O₂-induced cell death evaluated at 24 h in sipunculan celomocytes under normoxia and hypoxia and we also characterized the dose-effect profile of some early indicators of oxidative damage and antioxidant response. Marine coastal pollution often involves increased levels of heavy metals and pesticides that negatively impact the benthic communities. At the cellular level these pollutants often increase oxidative stress, causing altered cellular functions and eventually cell death. At the same time tidal flat habitats are transiently exposed to hypoxic conditions resulting from organic enrichment, algal bloom decomposition, and sediment movements in estuarine mudflats and litoral tidal flats (Lim *et al.*, 2006; Neira *et al.*, 2006). In fact, low-oxygen conditions are important in structuring the diversity and abundance of benthic communities (Van Colen *et al.*, 2010).

Our model of H₂O₂-induced cell death resembles a variety of cell injury situations caused by agents targeting the mitochondria. Many xenobiotics including several heavy metals and some pesticides target the mitochondria and cause increased intracellular production of ROS (Bagchi *et al.*, 2002). As shown above, a single pulse of H₂O₂ caused cell death at 24 h in a dose-dependent manner. However, the sigmoid shape of the curve indicated that a linear dose-dependent increase in cell death is present only at doses above EC30 corresponding to 1.0 mM H₂O₂. In addition the smooth slope of this linear phase of the dose-effect curve indicated that celomocytes were heterogeneous in their susceptibility to H₂O₂-induced cell death. The dose range, another indicator of variable susceptibility, was 0.6 mM-3.9 mM for EC10-EC90 indicating that some celomocytes may require up to 7 times more H₂O₂ than others to be killed.

The level of mitochondrial damage caused by the pulse of H₂O₂, as determined by the amount of cells with collapsed MMP, became stabilized after 3 h. Thus we explored the effect of a range of doses causing a known level of cell death at 24 h over some biomarkers of oxidative damage assessed at 3h post-exposure. Both the amount of cells with collapsed MMP and intracellular O₂⁻ production were increased after 3 h exposure in a dose dependent manner consistent with the idea that an increase in mitochondrial damage will cause an increase in intracellular ROS level.

GSH is the most abundant intracellular thiol and plays an essential role in maintaining the

intracellular redox environment (Meister and Anderson, 1983). The H₂O₂ dose-dependent decrease in GSH at 3 h indicated a widespread oxidation of thiols associated with increased intracellular ROS in an attempt to reduce the impact of oxidative damage. The negative correlations GSH level vs. O₂⁻, and GSH vs. cells with collapsed MMP confirmed this interpretation. Interestingly, a decrease in cellular GSH concentration has been reported to be an early event in the apoptotic cascade induced by death receptor activation, mitochondrial apoptotic signalling, drug exposure and oxidative stress (Circo and Aw, 2008). Thus, O₂⁻ production, the amount of cells with collapsed MMP and the reduction in GSH can all be used as early biomarkers of effect anticipating the amount of cell death caused by oxidative damage at 24h and could be of potential ecotoxicological usefulness (da Silva *et al.*, 1998).

The most abundant cells in the celomic fluid are hemerythrocytes which are involved in O₂ transport (above 75 %), while phagocytic cells with a diameter close to that of hemerythrocytes are the second largest cell type representing up to 25 % of celomocytes. This percentage figures apply to suspensions of celomocytes prepared under the conditions used in this study that exclude gonadal cells and two granular cell types designated large and small granular leukocytes (for a detailed description and discussion of cell types and relative proportions found in *T. petricola* and its comparison to other species of Sipuncula see (Blanco, 2010). We showed that phagocytes produced O₂⁻ after engulfment of zymosan, and that O₂⁻ level peaked at 1 h but decreased afterwards providing evidence of the occurrence of oxidative burst (Chang *et al.*, 2006; Xian *et al.*, 2010). Thus phagocytes should be well equipped to tolerate transient increases of intracellular ROS and may be more resistant to H₂O₂ than hemerythrocytes. The sigmoid shape of the cytotoxic H₂O₂ dose-effect curve showed that at lower doses the rate of change in cell death effect was low. We also observed that even though cell death rate was low in these samples, the net number of cells was decreased. We also noted that SSC was increased even with the lower doses and that MMP dose effect curve was less sigmoid and more linear in shape at low doses. Thus we speculated that phagocytes could be engulfing the more susceptible celomocytes that were killed at lower doses masking the true rate of dead cells. As shown in Figure 6, healthy phagocytes were able to engulf H₂O₂-treated cells causing them to increase their own SSC signal. Uptake of dead or dying cells should be important in the study of cell death in mixed populations where phagocytes may completely eliminate apoptotic cells before they can be detected by regular methods such as fluorescent Annexin-V labelling.

Paradoxically uptake of dead cells will be even more evident at low cytotoxic effect doses where the apoptotic phenotype is supposed to be more readily detected. In fact the finding of engulfed dead cells by resident macrophages has been underscored as a robust apoptotic indicator in tissues (Kroemer *et al.*, 2009). Exposure of phosphatidylserine is known as an "eat me" signal in eukaryotic cells and the phagocytosis of

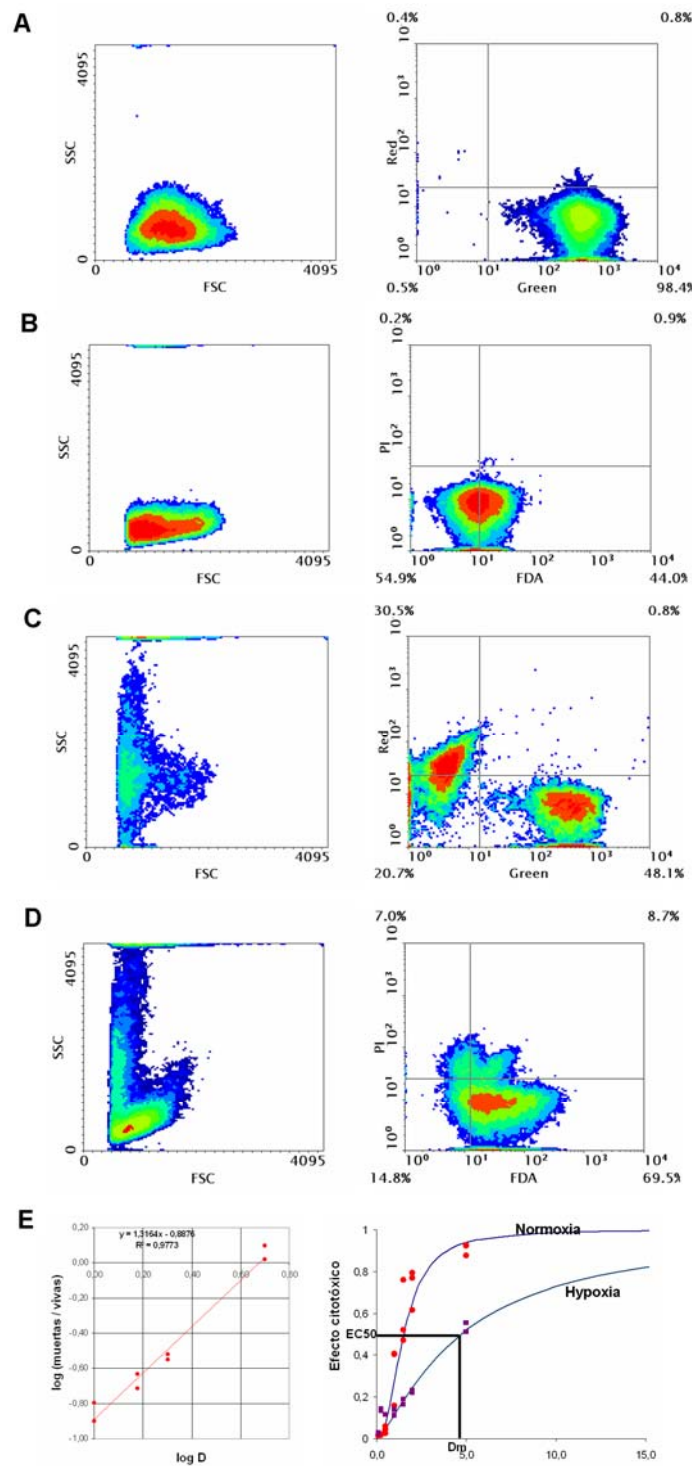


Fig. 7 Comparative effects of H₂O₂ under hypoxia and normoxia. A) Density plots showing FSC vs. SSC parameters (left) and FDA vs. PI (right) of untreated cells cultured for 24 h under normoxia at 18 °C. FDA fluorescence ranges between 100 and 1000 over a log scale. B) A similar set of density plots of untreated cells cultured for 24 h at 18 °C under hypoxia. FDA fluorescence is decreased to values around 10 in a log scale owing to strong pH decrease (Khodorov *et al.*, 1994). However viability remains the same as cells cultured in normoxia, as indicated by the complete exclusion of the PI probe (right plot). C) Density plots of cells treated with EC₅₀ H₂O₂ under normoxia. FDA fluorescence ranges between 100 and 1,000 in a log scale. D) Density plots of cells treated with EC₅₀ H₂O₂ under hypoxia. Viability remains high and FDA fluorescence is decreased although to a lesser extent than untreated cells shown in B). E) Calculation of EC₅₀ H₂O₂ in cells cultured under hypoxia applying a regression of log data and using the median effect equation (left). The slope and the intercept obtained were used to calculate the EC₅₀ (mean ± SE = 4.72 mM ± 0.31; N = 24) and the parameters of the dose-effect curve under hypoxia and compared to the curve obtained under normoxia (right). Red dots correspond to experimental values.

apoptotic cells may also contribute to eliminate the release of potentially harmful material including ROS production and intracellular pathogens (Birge and Ucker, 2008; Krysko and Vandenabeele, 2008).

We have already demonstrated in a previous work that H₂O₂ induces apoptotic cell death using several classical morphological and biochemical indicators of apoptotic death phenotype such as chromatin condensation, nuclear membrane rippling, cell membrane blebbing, DNA degradation to multiples of oligonucleosomal size, mitochondrial membrane depolarization and exposure of phosphatidylserine in the outer leaflet of the cell membrane (Blanco *et al.*, 2005). In the present study we did not address the question of whether H₂O₂ used at a fixed dose induces apoptosis or alternative forms of cell death but instead we evaluated how sensitive or resistant were celomocytes to H₂O₂ under hypoxia as compared to normoxia. Although apoptotic indicators are good measures of cell death phenotype they are not necessarily good measures of cell death rates to calculate EC50 dose. Many apoptotic indicators require the cells to be killed by fixation and even apoptotic cells detected by annexin V are often live as indicated by exclusion of PI. The amount of cells with complete collapse of MMP is even considered an early indicator of apoptosis and as shown in this study it does not provide a measure of cell death (Kroemer *et al.*, 2009). However, since the EC50 dose is also the minimal dose that kills at least 50 % of cells, it is not surprising that the death phenotype at the EC50 dose is often apoptosis or alternative forms of programmed cell death rather than passive necrosis.

Hypoxia causes increased ROS production and damage of lipids and proteins (Prabhakar *et al.*, 2007; Solaini *et al.*, 2010). Response to hypoxia is characterized by adaptive changes in the circulatory and hemopoietic systems and includes angiogenesis, vasodilation, and increased erythropoiesis, while expression of several enzymes and transporters are modified to enhance uptake and breakdown of glucose through anaerobic glycolysis. Since hypoxia increases ROS it may be anticipated that H₂O₂ will be more toxic under hypoxia. However, the assays conducted under hypoxia showed that the cytotoxic effect of H₂O₂ was diminished. The EC50 was increased from 1.5 mM to 4.7 mM. In addition, the range EC10-EC90 (0.6 mM - 3.9 mM under normoxia) was expanded to 0.9 mM - 25.1 mM under hypoxia indicating that variability was also increased and that the tolerance increase was exceedingly high in some particular cells.

Studies in other eukaryotes have demonstrated that hypoxia-induced mitochondrial ROS is part of the mechanism of O₂ sensing (Chandel *et al.*, 2000), and that antioxidant mechanisms are activated in concert with metabolic changes due to the activation of hypoxia inducing factor and upregulation of several genes (Gorr *et al.*, 2010). Thus the net result could be an increased tolerance to oxidative damage as we have observed in our study in sipunculans. The strong acidification of the celomocyte cytoplasm after 24 h hypoxia without showing any change in cell viability is consistent

with enhanced anaerobic metabolism and production of lactic acid. As said before sipunculans are oxyconformants but prolonged hypoxia ends up in anerobiosis with increased production of lactic acid. Interestingly, it has been suggested that the body wall with longitudinal and circular muscles is likely supplied with oxygen predominantly from sea water rather than from celomic fluid (Portner *et al.*, 1985). Thus, anaerobic metabolism in celomic fluid may be the main energy supply at low oxygen tension while some degree of aerobic respiration could still take place in the body wall. The tolerance of celomocytes to hypoxia, particularly of phagocytes which are critical cells of the innate immune response, and even their increased tolerance to oxidative stress in this condition could influence the ecological dominance of sipunculans together with polychaetes among the macrobenthos under conditions of oxygen deficiency.

References

- Amor A, López Armengol M, Iñiguez Rodriguez A, Traversa L. Intertidal endolithic fauna and its relationship to the mineralogical, physical and chemical characteristics of the substrate. *Mar. Biol.* 111: 271-280, 1991.
- Bagchi D, Balmoori J, Bagchi M, Ye X, Williams CB, Stohs SJ. Comparative effects of TCDD, endrin, naphthalene and chromium (VI) on oxidative stress and tissue damage in the liver and brain tissues of mice. *Toxicology* 175: 73-82, 2002.
- Birge RB, Ucker DS. Innate apoptotic immunity: the calming touch of death. *Cell Death Differ.* 15: 1096-102, 2008.
- Blanco G. Cell death and the immune responses of the sipunculan worm *Themiste petricola*. *Inv. Surv. J.* 7: 239-250, 2010.
- Blanco GA, Bustamante J, Garcia M, Hajos SE. Hydrogen peroxide induces apoptotic-like cell death in celomocytes of *Themiste petricola* (Sipuncula). *Biol. Bull.* 209: 168-83, 2005.
- Cadenas E, Davies KJ. Mitochondrial free radical generation, oxidative stress, and aging. *Free Radic. Biol. Med.* 29: 222-30, 2000.
- Cantoni O, Cattabeni F, Stocchi V, Meyn RE, Cerutti P, Murray D. Hydrogen peroxide insult in cultured mammalian cells: relationships between DNA single-strand breakage, poly(ADP-ribose) metabolism and cell killing. *Biochim. Biophys. Acta* 1014: 1-7, 1989.
- Cavaliere V, Papademetrio DL, Alvarez EM, Blanco GA. Haemostatic and immune role of cellular clotting in the sipunculan *Themiste petricola*. *Cell Tissue Res.* 339: 597-611, 2010.
- Circu ML, Aw TY. Glutathione and apoptosis. *Free Radic. Res.* 42: 689-706, 2008.
- Comhair SA, Erzurum SC. Antioxidant responses to oxidant-mediated lung diseases. *Am. J. Physiol. Lung Cell. Mol. Physiol.* 283: 246-55, 2002.
- Cutler EB. The Sipuncula: their systematics, biology, and evolution, Comstock Pub. Associates, Ithaca, 1994.
- Chandel NS, Maltepe E, Goldwasser E, Mathieu CE, Simon MC, Schumacker PT. Mitochondrial reactive oxygen species trigger hypoxia-induced transcription. *Proc. Natl. Acad. Sci. USA* 95: 11715-11720, 1998.

- Chandel NS, McClintock DS, Feliciano CE, Wood TM, Melendez JA, Rodriguez AM, *et al.* Reactive oxygen species generated at mitochondrial complex III stabilize hypoxia-inducible factor-1 α during hypoxia: a mechanism of O₂ sensing. *J. Biol. Chem.* 275: 25130-25138, 2000.
- Chang CC, Lee PP, Liu CH, Cheng W. Trichlorfon, an organophosphorus insecticide, depresses the immune responses and resistance to *Lactococcus garvieae* of the giant freshwater prawn *Macrobrachium rosenbergii*. *Fish Shellfish Immunol.* 20: 574-585, 2006.
- Chen Y, Azad MB, Gibson SB. Superoxide is the major reactive oxygen species regulating autophagy. *Cell Death Differ.* 16: 1040-1052, 2009.
- Chora S, McDonagh B, Sheehan D, Starita-Geribaldi M, Romeo M, Bebianno MJ. Ubiquitination and carbonylation as markers of oxidative-stress in *Ruditapes decussatus*. *Mar. Environ. Res.* 66: 95-97, 2008.
- Chou TC. The mass-action law based algorithm for cost-effective approach for cancer drug discovery and development. *Am. J. Cancer Res.* 1: 925-954, 2011.
- da Silva EM, Soares AM, Moreno AJ. The use of the mitochondrial transmembrane electric potential as an effective biosensor in ecotoxicological research. *Chemosphere* 36: 2375-2390, 1998.
- Duranteau J, Chandel NS, Kulisz A, Shao Z, Schumacker PT. Intracellular signaling by reactive oxygen species during hypoxia in cardiomyocytes. *J. Biol. Chem.* 273: 11619-24, 1998.
- Edmonds S. The respiratory metabolism of *Dendrostomum cymodoceae* Edmonds (Sipunculoidea). *Aust. J. Mar. Freshwat. Res.* 8: 55-63, 1957.
- Fuller-Espie S, Nacarelli T, Blake E, Bearoff F. The effect of oxidative stress on phagocytosis and apoptosis in the earthworm *Eisenia hortensis*. *Inv. Surv. J.* 7: 89-106, 2010.
- Geisow MJ. Fluorescein conjugates as indicators of subcellular pH. A critical evaluation. *Exp. Cell Res.* 150: 29-35, 1984.
- Gorr TA, Wichmann D, Hu J, Hermes-Lima M, Welker AF, Terwilliger N, *et al.* Hypoxia tolerance in animals: biology and application. *Physiol. Biochem. Zool.* 83: 733-752, 2010.
- Hyman L. The protostomatous coelomates - Phylum Sipunculida, Chapter XXII, The celomate Bilateria, vol V. McGraw Hill, New York, pp 610-696, 1959.
- Jiang L, Liu Y, Ma MM, Tang YB, Zhou JG, Guan YY. Mitochondria dependent pathway is involved in the protective effect of bestrophen-3 on hydrogen peroxide-induced apoptosis in basilar artery smooth muscle cells. *Apoptosis* 18: 556-565, 2013.
- Khodorov B, Valkina O, Turovetsky V. Mechanisms of stimulus-evoked intracellular acidification in frog nerve fibres. *FEBS Lett.* 341: 125-127, 1994.
- Koppenol WH. The Haber-Weiss cycle--70 years later. *Redox Rep.* 6: 229-234, 2001.
- Kristof A, Wollesen T, Wanninger A. Segmental mode of neural patterning in sipuncula. *Curr. Biol.* 18: 1129-1132, 2008.
- Kroemer G, Galluzzi L, Vandenabeele P, Abrams J, Alnemri ES, Baehrecke EH, *et al.* Classification of cell death: recommendations of the Nomenclature Committee on Cell Death 2009. *Cell Death Differ.* 16: 3-11, 2009.
- Krysko DV, Vandenabeele P. From regulation of dying cell engulfment to development of anti-cancer therapy. *Cell Death Differ.* 15: 29-38, 2008.
- Le Meur N, Rossini A, Gasparetto M, Smith C, Brinkman RR, Gentleman R. Data quality assessment of ungated flow cytometry data in high throughput experiments. *Cytometry A* 71: 393-403, 2007.
- Lim HS, Diaz RJ, Hong JS, Schaffner LC. Hypoxia and benthic community recovery in Korean coastal waters. *Mar. Pollut. Bull.* 52: 1517-1526, 2006.
- Lombardo T, Anaya L, Kornblihtt L, Blanco G. Median Effect Dose and Combination Index Analysis of Cytotoxic Drugs Using Flow Cytometry, vol. Chapter 20. Intech Open Publisher Rijeka, Croatia, 2012.
- Lombardo T, Cavaliere V, Costantino SN, Kornblihtt L, Alvarez EM, Blanco GA. Synergism between arsenite and proteasome inhibitor MG132 over cell death in myeloid leukaemic cells U937 and the induction of low levels of intracellular superoxide anion. *Toxicol. Appl. Pharmacol.* 258: 351-366, 2011.
- Luo X, Chen B, Zheng R, Lin P, Li J, Chen H. Hydrogen peroxide induces apoptosis through the mitochondrial pathway in rat Schwann cells. *Neurosci. Lett.* 485: 60-64, 2010.
- Lushchak VI, Bagnyukova TV. Hypoxia induces oxidative stress in tissues of a goby, the rotan *Percottus glenii*. *Comp. Biochem. Physiol.* 148B: 390-7, 2007.
- Martin M, Lindqvist L. The pH dependence of fluorescein fluorescence. *J. Luminescence* 10: 381-390, 1975.
- McDonagh B, Sheehan D. Effects of oxidative stress on protein thiols and disulphides in *Mytilus edulis* revealed by proteomics: actin and protein disulphide isomerase are redox targets. *Mar. Environ. Res.* 66: 193-195, 2008.
- Meister A, Anderson ME. Glutathione. *Annu. Rev. Biochem.* 52: 711-760, 1983.
- Meyer A, Lieb B. Respiratory proteins in *Sipunculus nudus*--implications for phylogeny and evolution of the hemerythrin family. *Comp. Biochem. Physiol.* 155B: 171-7, 2010.
- Miller EW, Dickinson BC, Chang CJ. Aquaporin-3 mediates hydrogen peroxide uptake to regulate downstream intracellular signaling. *Proc. Natl. Acad. Sci. USA* 107: 15681-15686, 2010.
- Neira C, Grosholz ED, Levin LA, Blake R. Mechanisms generating modification of benthos following tidal flat invasion by a *Spartina hybrid*. *Ecol. Appl.* 16: 1391-404, 2006.
- Palomba L, Sestili P, Columbaro M, Falcieri E, Cantoni O. Apoptosis and necrosis following exposure of U937 cells to increasing concentrations of hydrogen peroxide: the effect

- of the poly(ADP-ribose)polymerase inhibitor 3-aminobenzamide. *Biochem. Pharmacol.* 58: 1743-1750, 1999.
- Payne JL, McClain CR, Boyer AG, Brown JH, Finnegan S, Kowalewski M, *et al.* The evolutionary consequences of oxygenic photosynthesis: a body size perspective. *Photosynth. Res.* 107: 37-57, 2011.
- Peng Y, Yuan G, Overholt JL, Kumar GK, Prabhakar NR. Systemic and cellular responses to intermittent hypoxia: evidence for oxidative stress and mitochondrial dysfunction. *Adv. Exp. Med. Biol.* 536: 559-564, 2003.
- Portner HO, Heisler N, Grieshaber MK. Oxygen consumption and mode of energy production in the intertidal worm *Sipunculus nudus* L.: definition and characterization of the critical PO₂ for an oxyconformer. *Respir. Physiol.* 59: 361-377, 1985.
- Prabhakar NR, Kumar GK, Nanduri J, Semenza GL. ROS signaling in systemic and cellular responses to chronic intermittent hypoxia. *Antioxid Redox Signal* 9: 1397-1403, 2007.
- Sarkar A, Mandal G, Singh N, Sundar S, Chatterjee M. Flow cytometric determination of intracellular non-protein thiols in *Leishmania promastigotes* using 5-chloromethyl fluorescein diacetate. *Exp. Parasitol.* 122: 299-305, 2009.
- Schulze A, Rice ME. Musculature in sipunculan worms: ontogeny and ancestral states. *Evol. Dev.* 11: 97-108, 2009.
- Sheehan D, McDonagh B. Oxidative stress and bivalves: a proteomic approach. *Inv. Surv. J.* 5: 110-123, 2008.
- Solaini G, Baracca A, Lenaz G, Sgarbi G. Hypoxia and mitochondrial oxidative metabolism. *Biochim. Biophys. Acta* 1797: 1171-1177, 2010.
- Speakman JR, Selman C. The free-radical damage theory: Accumulating evidence against a simple link of oxidative stress to ageing and lifespan. *Bioessays* 33: 255-259, 2011.
- Sperling EA, Frieder CA, Raman AV, Girguis PR, Levin LA, Knoll AH. Oxygen, ecology, and the Cambrian radiation of animals. *Proc. Natl. Acad. Sci. USA* 110: 13446-13451, 2013.
- Valavanidis A, Vlahogianni T, Dassenakis M, Scoullou M. Molecular biomarkers of oxidative stress in aquatic organisms in relation to toxic environmental pollutants. *Ecotoxicol. Environ. Saf.* 64: 178-189, 2006.
- Valko M, Leibfritz D, Moncol J, Cronin MT, Mazur M, Telser J. Free radicals and antioxidants in normal physiological functions and human disease. *Int. J. Biochem. Cell. Biol.* 39: 44-84, 2007.
- Van Colen C, Montserrat F, Vincx M, Herman PM, Ysebaert T, Degraer S. Long-term divergent tidal flat benthic community recovery following hypoxia-induced mortality. *Mar. Pollut. Bull.* 60: 178-186, 2010.
- Wang J, Wang Q, Li J, Shen Q, Wang F, Wang L. Cadmium induces hydrogen peroxide production and initiates hydrogen peroxide-dependent apoptosis in the gill of freshwater crab, *Sinopotamon henanense*. *Comp. Biochem. Physiol.* 156C: 195-201, 2012.
- Wood JG, Johnson JS, Mattioli LF, Gonzalez NC. Systemic hypoxia promotes leukocyte-endothelial adherence via reactive oxidant generation. *J. Appl. Physiol.* (1985) 87: 1734-1740, 1999.
- Xian JA, Wang AL, Ye CX, Chen XD, Wang WN. Phagocytic activity, respiratory burst, cytoplasmic free-Ca⁽²⁺⁾ concentration and apoptotic cell ratio of haemocytes from the black tiger shrimp, *Penaeus monodon* under acute copper stress. *Comp. Biochem. Physiol.* 152C: 182-8, 2010.
- Zhang Y, Marcillat O, Giulivi C, Ernster L, Davies KJ. The oxidative inactivation of mitochondrial electron transport chain components and ATPase. *J. Biol. Chem.* 265: 16330-16336, 1990.